Earth and Planetary Science Letters 500 (2018) 136–144

Contents lists available at ScienceDirect

Earth and Planetary Science Letters

www.elsevier.com/locate/epsl

Weathering dynamics reflected by the response of riverine uranium isotope disequilibrium to changes in denudation rate

Laifeng Li [a], Jun Chen [a], Tianyu Chen [a], Yang Chen [a], David William Hedding [b], Gen Li [c], Le Li [a], Tao Li [a], Laura F. Robinson [d], A. Joshua West [e], Weihua Wu [a], Chen-Feng You [f], Liang Zhao [a], Gaojun Li [a,*]

[a] MOE Key Laboratory of Surficial Geochemistry, Department of Earth and Planetary Sciences, Nanjing University, Nanjing 210023, China
[b] Department of Geography, University of South Africa, Pioneer Avenue, Florida 1710, South Africa
[c] Department of Earth, Planetary, and Space Sciences, University of California Los Angeles, Los Angeles, CA 90095, USA
[d] Bristol Isotope Group, School of Earth Sciences, University of Bristol, Bristol, UK
[e] Department of Earth Sciences, University of Southern California, 3651 Trousdale Parkway, Los Angeles, CA 90089, USA
[f] Earth Dynamic System Research Center, National Cheng Kung University, Tainan 701, Taiwan

ARTICLE INFO

Article history:
Received 15 February 2018
Received in revised form 2 August 2018
Accepted 4 August 2018
Available online 22 August 2018
Editor: D. Vance

Keywords:
erosion
soil
carbon cycle
landscape evolution
critical zone

ABSTRACT

The ratio between the activity of dissolved ^{234}U and ^{238}U in river water, $(^{234}U/^{238}U)_{Riv}$, shows promise for tracing weathering processes. It has been suggested that preferential ^{234}U release generates a high $(^{234}U/^{238}U)_{Riv}$ under low weathering intensity while congruent weathering, as expected for high weathering intensity, would release uranium with a secular equilibrium $(^{234}U/^{238}U)_{Riv}$ of 1. However, weathering intensity depends on the combination of exposure age of weathering interfaces and dissolution rate, complicating the use of $(^{234}U/^{238}U)_{Riv}$ as a tool in weathering studies. This work attempts to resolve the weathering dynamics reflected by $(^{234}U/^{238}U)_{Riv}$ using catchment scale denudation rate (D) as a first order approximation for the age of weathering interfaces. A global dataset ($n = 653$), including 132 new measurements from Chinese catchments, indicates changing responses of $(^{234}U/^{238}U)_{Riv}$ to D. Higher values (>1.5) and larger variability of $(^{234}U/^{238}U)_{Riv}$ are observed in catchments both with high (>3 mm/yr) and low D (<0.1 mm/yr). In contrast, the lowest values (approaching secular equilibrium) and the least variable $(^{234}U/^{238}U)_{Riv}$ are associated with catchments of medium to high D (0.3–2 mm/yr). The observed pattern can be explained by a model that involves competing uranium release from active- and inactive-weathering interfaces in response to a shifting weathering regime, from kinetically-limited to supply-limited. $(^{234}U/^{238}U)_{Riv}$ decreases with decreasing D under a kinetically-limited weathering regime due to the increasing contribution of congruent weathering relative to the preferential dissolution of ^{234}U from radioactively damaged sites as D decreases. In contrast, $(^{234}U/^{238}U)_{Riv}$ increases with decreasing D under a supply-limited weathering regime because the minerals that remain under these conditions continue to release ^{234}U to solution by recoil, while contributing little to the dissolved ^{238}U because of their slow dissolution rate. A much deeper depth of the weathering interface is suggested for catchments with high D due to higher weathering contribution from deep fractures relative to the poorly developed surface regolith. A young age of ~10 kyrs is constrained by the model for complete dissolution of exposed weathering-active minerals, which implies a rapid shifting from kinetically-limited to supply-limited weathering regime and limited influence of weathering on the calculation of comminution age based on $(^{234}U/^{238}U)$ in sediments. A site-specific dissolution rate that is consistent with those estimated from weathering profiles is also constrained, which suggests that the discrepancy between field and laboratory weathering rate may largely be controlled by the difference in chemical affinity associated with stagnant micro-pores, low permeability, and high rock/fluid ratios rather than the passivation of weathering interfaces.

1. Introduction

The significant roles that weathering plays in the Earth system, such as supplying nutrients to terrestrial and marine ecosys-

* Corresponding author.
E-mail address: ligaojun@nju.edu.cn (G. Li).

https://doi.org/10.1016/j.epsl.2018.08.008

tems (Cermeño et al., 2015), regulating the long-term balance of the global carbon cycle and geothermostat (Berner et al., 1983), and triggering climatic changes associated with tectonic uplift (Raymo et al., 1988), require a deep understanding of the factors that control weathering flux (e.g., Bluth and Kump, 1994; Jacobson et al., 2003; Li et al., 2016; Maher and Chamberlain, 2014; Riebe et al., 2004). The uranium isotope activity ratio of dissolved weathering products has been used to better understand weathering processes (e.g., Bourdon et al., 2009; Chabaux et al., 2001; Dosseto et al., 2006; Maher et al., 2006). Natural waters are enriched in ^{234}U relative to bedrock (Chabaux et al., 2003; Dunk et al., 2002) that is typically characterized by a secular equilibrium where the activity of ^{234}U ($\lambda_{234}{}^{234}U$, λ_{234} is decay constant) is equal to that of ^{238}U ($\lambda_{238}{}^{238}U$), such that the activity ratio ($^{234}U/^{238}U$) is 1. Laboratory experiments indicate that the enrichment of ^{234}U in natural waters can be attributed to both (1) the direct recoil ejection of the ^{234}U precursor during alpha decay of ^{238}U and (2) the preferential dissolution of radioactively damaged lattice sites that hold the ^{234}U nucleus (Andersen et al., 2009; Fleischer, 1980; Kigoshi, 1971). The relative contribution of recoil ejection and preferential dissolution is high when the supply of fresh mineral surfaces is abundant, resulting in preferential loss of ^{234}U to solution. On the other hand, congruent weathering would generate weathering products with a uranium isotope activity ratio approaching secular equilibrium (e.g., Maher et al., 2006; Pogge Von Strandmann and Henderson, 2015; Robinson et al., 2004a; Vigier, 2001). It is thus expected that the dissolved riverine uranium isotope activity ratio, $(^{234}U/^{238}U)_{Riv}$, is controlled by the age of the weathering interface (i.e., the weathering front) and the weathering rate that collectively determine weathering intensity.

The possible control of weathering intensity on $(^{234}U/^{238}U)_{Riv}$ (Pogge Von Strandmann and Henderson, 2015; Robinson et al., 2004a; Vigier et al., 2006) may help to resolve debates related to weathering limitation regimes and thus elucidate the relative importance of tectonics and climate on the global chemical weathering flux (Bluth and Kump, 1994; Ferrier et al., 2016; Hilley et al., 2010; Jacobson et al., 2003; Riebe et al., 2004; West et al., 2005). Under a low denudation rate (D), mineral residence time in the weathering zone is relatively long and weathering-active minerals can be completely dissolved before leaving the eroding surface. Under these conditions, it has been conceptually accepted that the chemical weathering rate (W) is limited by the supply of fresh minerals (supply-limited) and is thus linearly related to D (Riebe et al., 2004; West et al., 2005). Notably, such supply-limited weathering regimes provide the main premise for the "uplift-weathering" hypothesis which proposes that uplift-enhanced erosion promoted silicate chemical weathering and accelerated the drawdown of atmospheric CO_2 during the late Cenozoic (Raymo et al., 1988). In contrast, when ample fresh minerals are constantly produced under high D, W is limited by weathering reaction kinetics determined by factors such as rock type, temperature, supply of reactive fluid, and thus the flux becomes decoupled from D, i.e., "kinetically-limited" (West et al., 2005). A kinetically-limited weathering regime enables a negative feedback between atmospheric CO_2 concentration (and thus climate) and weathering rate, which is essential for silicate weathering to act as a geothermostat that maintains the balance of the carbon cycle and the habitability of the Earth (Berner et al., 1983; Li and Elderfield, 2013).

The proof of shifting weathering regimes, which generally relies on the relationship between W and D in modern weathering environments (Ferrier et al., 2016; Gabet and Mudd, 2009; West et al., 2005), is, however, elusive. Generally, a strong correlation can be observed between D and W under low D (West et al., 2005), but debate arises under high D. Results based on small granitic catchments show decoupling between D and W at high D (West et al., 2005), while compilation of global soil data suggests that W retains a tight coupling with D even at extremely high D (Larsen et al., 2014), challenging the existence of a true kinetically-limited weathering regime. A pure supply-limited weathering regime would require strong control of climate on D in order to sustain a stabilizing geothermostat (Ferrier et al., 2016), yet evidence for a strong climate control on denudation remains incomplete (Perron, 2017). In threshold landscapes, mass wasting (movement) is the major agent of erosion (Li et al., 2017a), and rapid incipient weathering of fresh slope debris may contribute to the high W at high D (Emberson et al., 2016), though much of this flux may not be from the silicate sources that consume atmospheric CO_2 over geological timescales (Jacobson et al., 2003), complicating the interpretation and implications for the carbon cycle. It is also possible that D and W are spuriously correlated since the calculation of W from soils, which is based on the chemical depletion of regolith, involves D. Moreover, W and D deduced from the dissolved and suspended flux of rivers both depend on runoff. In both cases, there is the risk of false correlation (Ferrier et al., 2016).

To avoid spurious correlation between D and W, weathering intensity as measured by proxies such as chemical depletion fraction (Ferrier et al., 2016) and lithium isotopic compositions (Dellinger et al., 2015) can be used as alternative indicators for shifting weathering limitation regimes. Supply limitation implies total dissolution of weathering-active minerals so that the same high degree of chemical depletion would be expected, while kinetic weathering limitation predicts a lower chemical depletion fraction at higher D due to restricted weathering time. While chemical depletion can be measured at single locations in hillslope regolith (e.g., Larsen et al., 2014; Riebe et al., 2004), it is difficult to make these measurements over large spatial scales that integrate weathering across the Earth's surface. Given the limited tools to infer weathering regime at the scale of river basins, the question is whether the $(^{234}U/^{238}U)$ in the dissolved load can help to make this distinction and provide quantitative information about weathering conditions under each regime.

If measurements of $(^{234}U/^{238}U)_{Riv}$ can further be used to constrain weathering rates, the resulting site-specific rates may also help to explain the 3–6 order of magnitude discrepancy between observations of dissolution rates in the field versus the laboratory (White and Brantley, 2003; White and Buss, 2014). Despite the relatively well established kinetics of mineral dissolution in the laboratory (Brantley and Olsen, 2014), this large discrepancy inhibits extrapolation of experimentally-based kinetic laws to field settings, hampering efforts to quantify the strength of feedbacks between climate and silicate weathering (Li et al., 2016; Maher and Chamberlain, 2014). Both intrinsic and extrinsic processes have been invoked to explain the lab-to-field rate discrepancy (White and Brantley, 2003). The intrinsic factors could include overestimation of the active weathering surface caused by coating of secondary precipitates and consumption of energetically active surface. The extrinsic factors are related to differences in chemical affinity of the reacting fluid due to the stagnant micro pores, slow flow rate, and high rock/fluid ratio in the field. The site-specific dissolution rate constrained by uranium isotope disequilibrium, which is independent of estimated active surface area (Maher et al., 2006), may be used to differentiate between intrinsic and extrinsic factors because the intrinsic factors would not influence site-specific dissolution rates.

Though promising for untangling these complicated questions about weathering, dissolved riverine uranium isotope activity ratios vary widely, and their relationship with weathering intensity appears complex. High $(^{234}U/^{238}U)_{Riv}$ has been observed in some catchments flowing toward the east coast of the South Island, New Zealand, where a kinetically-limited weathering regime and associ-

ated low weathering congruency are suggested due to high erosion rates (Robinson et al., 2004a). However, Himalayan rivers and the rivers flowing to the west coast of the South Island, New Zealand, where extremely high erosion rates have also been observed, show unexpectedly low $(^{234}U/^{238}U)_{Riv}$ approaching the equilibrium value (Chabaux et al., 2001; Robinson et al., 2004a). High $(^{234}U/^{238}U)_{Riv}$ values are also reported in catchments with low erosion rates, such as the Orange River in South Africa and the rivers draining the Siberian Traps (Bagard et al., 2011; Kronfeld and Vogel, 1991). More importantly, the increasing $(^{234}U/^{238}U)_{Riv}$ with decreasing D in Iceland is counterintuitive to the control of weathering intensity on $(^{234}U/^{238}U)_{Riv}$ (Vigier et al., 2006).

To better understand how weathering dynamics might be reflected by $(^{234}U/^{238}U)_{Riv}$, this work compiles a global dataset from catchments with known D, including new measurements from Chinese rivers. It is generally accepted that higher D is associated with shorter residence duration of regolith (Heimsath et al., 1997). Thus, catchment scale D may be used as an independent constraint on the age of weathering interfaces. On this basis, a model is developed to explain the responses of $(^{234}U/^{238}U)_{Riv}$ to changing D considering the influences of shifting weathering regime and site-specific dissolution rates. Implications for understanding weathering regimes, site-specific dissolution rates, and the influence of weathering on the calculation of sediment comminution ages are then discussed.

2. Method and data compilation

River water samples were collected from small catchments on the Tibetan Plateau and Taiwan Island (Supplementary Table S1). Most of these samples were taken during the summer monsoon season. Some of these samples were also taken in the dry winter season. The changes between the two water stages are relatively small (Table S2). Extensive research in these regions has produced a large dataset of catchment scale denudation rates based on ^{10}Be concentration and sediment flux (see supplementary Table S2). The sampling locations were designed to be at or near the sites where the catchment denudation rate was constrained. The sampled catchments have a wide range of D from 0.012 mm/yr to 9.9 mm/yr. The lithologies are mainly granite and meta-sediment on the Tibetan Plateau and meta-sediment on Taiwan.

Approximately one liter of water was taken for each sample. The samples were filtered using 0.22 μm cellulose acetate membrane filters and then acidified to pH = 2 using droplets of 15 M HNO_3 in the field. About 30–50 ml splits of the samples were evaporated in a clean laboratory to concentrate the solutes. Concentrated HCl acid was added to the samples to avoid adsorption and co-precipitation during evaporation. Uranium in the concentrated sample was purified using UTEVA resin (Wang and You, 2013). Measurements of $^{234}U/^{238}U$ ratios were made on a MC-ICP-MS (Neptune Plus) at the MOE Key Laboratory of Surficial Geochemistry, Department of Earth and Planetary Sciences, Nanjing University. Instrumental bias between ^{234}U and ^{238}U was corrected by normalizing the $^{238}U/^{235}U$ ratio to 137.84, and then a standard sample bracketing (SSB) method, using a NJU-U (Nanjing University Uranium) standard that was previously calibrated to IRMM3184 (Li et al., 2017b), was applied to correct the short-term variation of the 'gain' between the Faraday cup and secondary electron multiplier (SEM) that collect the ^{238}U and ^{234}U, respectively. Finally, the $(^{234}U/^{238}U)$ value was calculated using the ratio between the measured $^{234}U/^{238}U$ ratio and the equilibrium ratio of $\lambda_{238}/\lambda_{234}$ with the decay constant $\lambda_{234} = 2.82206 \times 10^{-6}$ yr^{-1} (Cheng et al., 2013), and $\lambda_{238} = 1.55125 \times 10^{-10}$ yr^{-1} (Jaffey et al., 1971). The mean of complete procedural blanks measured by counting the ^{238}U signal was about 2 pg, which is below 0.1% of the measured sample amount. Repeated measurements of standard seawater IAPSO using the whole sample processing procedure give a long-term $(^{234}U/^{238}U)$ value of 1.143 ± 0.004 (2 × external standard deviation, $n = 20$), which is consistent with the recommended value of 1.144 ± 0.004 (Wang and You, 2013) and open ocean seawater of approximately 1.147 (Andersen et al., 2010; Robinson et al., 2004b).

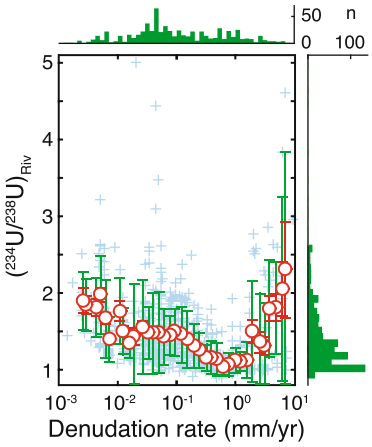

Fig. 1. Compilation of dissolved $(^{234}U/^{238}U)$ from global rivers with known denudation rates (D). Data sources can be found in Table S2. Each data point is depicted using a cross. The circles with error bars show the average value within each ±0.1 bin at every 0.1 step of log(D). Green error bars show the standard deviation and red error bars are the standard error (standard deviation of the mean). The histograms beside the axis indicate data distribution.

The $(^{234}U/^{238}U)_{Riv}$ values, including the new Chinese measurements, have been collated into a global dataset. For the purpose of this study, only the rivers with reliable denudation rates, derived either from ^{10}Be concentration, or from the suspended and dissolved yields, were used. The $(^{234}U/^{238}U)_{Riv}$ data was compiled from 53 published articles. Details on the data sources and the corresponding denudation rate data can be found in Table S2. For rivers where multiple measurements were made at different sampling periods, average values and external standard deviation (std) of those data were used. When calculating the catchment denudation rate from the total suspended sediment (TSS) and the total dissolved solid (TDS), a density of 2700 kg/m^3 was used. Catchments that drain uranium mines were excluded because of the complicated influences uranium mines have on the $(^{234}U/^{238}U)_{Riv}$. Details of the global data compilation, including data sources, can be found in Table S2.

3. Results

In total, 653 $(^{234}U/^{238}U)_{Riv}$ catchments were compiled into the global dataset, including 132 new measurements from Chinese rivers. The D of the compiled catchments ranges from 0.0014 mm/yr to 9.9 mm/yr with a lognormal distribution (Fig. 1). The compiled $(^{234}U/^{238}U)_{Riv}$ values show significant variability with a minimum value slightly less than 1 and a maximum value reaching up to 5. The distribution of the compiled $(^{234}U/^{238}U)_{Riv}$ is highly skewed toward the equilibrium value of 1 (Fig. 1).

In general, a U-shaped relationship can be observed between $(^{234}U/^{238}U)_{Riv}$ and D (Fig. 1). This overall relationship is much clearer when the $(^{234}U/^{238}U)_{Riv}$ data is averaged by 0.1 log(D) steps with ±0.1 log(D) bin width (Fig. 1). Catchments with high and low D have higher $(^{234}U/^{238}U)_{Riv}$ values than catchments with medium-high D. The lowest $(^{234}U/^{238}U)_{Riv}$ values, which approach equilibrium, are associated with catchments that exhibit a D of ~0.6 mm/yr. Variability of $(^{234}U/^{238}U)_{Riv}$, as illustrated by standard deviation of each data bin, also shows clear dependence on D; much higher variability of $(^{234}U/^{238}U)_{Riv}$ values is observed for

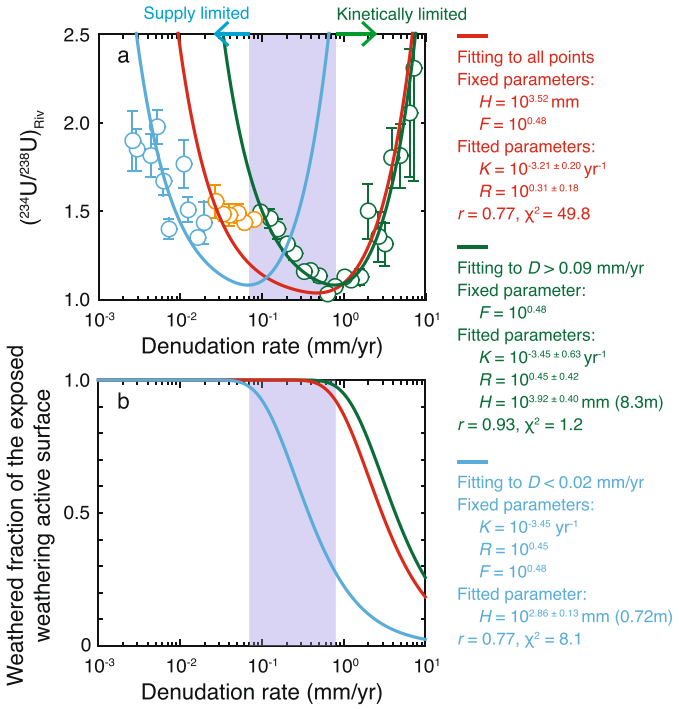

Fig. 2. (a) Fitting the relationship between $(^{234}U/^{238}U)_{Riv}$ and denudation rate (D) to the model, i.e., Eq. (9), based on average $(^{234}U/^{238}U)_{Riv}$ for binned values of D in the global dataset. Error bars show the standard deviation of the mean. The least square method is used to find the best fit. (b) The changing weathered fraction of the exposed weathering-active surface (f_W) as a function of D is indicated using the modeled parameters in (a).

catchments with high and low D. The decreasing $(^{234}U/^{238}U)_{Riv}$ associated with decreasing D for catchments with $D > 0.6$ mm/yr is rather steep (Fig. 2). In contrast, the increasing $(^{234}U/^{238}U)_{Riv}$ associated with decreasing D for catchments with $D < 0.6$ mm/yr is discontinuous, particularly at D values between 0.02 mm/yr and 0.09 mm/yr, and shows a somewhat weaker relationship compared to the decrease in $(^{234}U/^{238}U)_{Riv}$ for $D > 0.6$ mm/yr.

4. Discussion

4.1. Model interpretation

4.1.1. Importance of weathering-inactive minerals

The changing dependence of $(^{234}U/^{238}U)_{Riv}$ on D is different from the expected trend of decreasing $(^{234}U/^{238}U)_{Riv}$ with increasing weathering intensity, as predicted if completely congruent weathering of all U-containing minerals generates a constant, near-to-equilibrium $(^{234}U/^{238}U)_{Riv}$ at low D (Andersen et al., 2009; Vigier, 2001). Instead, $(^{234}U/^{238}U)$ is elevated above secular equilibrium at the lowest D in the dataset. We propose that the changing responses of $(^{234}U/^{238}U)_{Riv}$ to D results from the competing release of uranium between weathering-active and weathering-inactive surfaces that respond differently to changing weathering intensity. Once the weathering-active surfaces have been consumed, the weathering-inactive surfaces continue to release ^{234}U by alpha recoil, but they release little ^{238}U because of their slow dissolution rates. The amount of recoil-ejected ^{234}U increases with longer mineral residence time, increasing the $(^{234}U/^{238}U)_{Riv}$ as D decreases. This interpretation requires a significant fraction of U in weathering-inactive minerals. As previous research has shown (Bosia et al., 2018), quartz, rutile, zircon, titanite and monazite (all generally resistant to dissolution) collectively contribute about 70% of the uranium load of Himalayan rivers, indicating the important role of weathering-inactive minerals in the U budget.

4.1.2. Model

A model can be developed to illustrate the influence of competing uranium release from weathering-active and weathering-inactive surfaces on $(^{234}U/^{238}U)_{Riv}$ (Fig. 2a). The assumption of a weathering steady state is adopted so that the average $(^{234}U/^{238}U)$ value of weathering solutes contributed from various regolith depths is equal to the cumulative $(^{234}U/^{238}U)$ value of U released by the eroding materials, i.e., the different weathering stages of minerals in the contemporary regolith can be regarded as a reflection of weathering history of the eroding materials. Decay of the released ^{234}U and ^{238}U in the water are ignored in this study due to the short residence time of water in the catchments (~yrs, Jasechko et al., 2017), although in some cases significant inputs of old (> thousand years) groundwater could occur, which might influence the model results but are not needed to describe the first-order trends in the data.

The weathering-inactive fraction does not release ^{234}U and ^{238}U via weathering but can eject ^{234}U through the recoiling effect associated with the alpha-decay of ^{234}Th (the parent nuclide of ^{234}U). A geometric calculation has shown that one quarter of the daughter ^{234}U nuclei produced by the alpha decay of ^{238}U within the recoiling distance of a mineral surface can be ejected (Kigoshi, 1971). Thus, the cumulative recoil-associated release of ^{234}U ($^{234}A_{IA}$, with dimensional unit symbol of N) from a given exposed weathering-inactive surface can be expressed as:

$$^{234}A_{IA} = dS_{IA}C_{IA}\lambda_{238}T_W/4 \quad (1)$$

where d (L) is the α-recoil distance of ^{234}Th; S_{IA} (L^2) is area of the weathering-inactive surface; C_{IA} (N/L^3) is volumetric molar concentration of ^{238}U of the exposed inactive minerals; and T_W (T) represents the mean surface exposure age of the eroding materials.

In the case of weathering-active minerals, excess ^{234}U can come both from recoil, which will be included in bulk dissolution in eq. (4), and loss during dissolution of damaged sites at the mineral surface. Preferential dissolution of ^{234}U from the radioactively damaged sites on the weathering-active surface is assumed to be rapid and complete considering the much higher dissolution rate of uncrystallized glass (similar to the damaged sites) compared to crystals of similar chemical composition (Brantley and Olsen, 2014). Preferential dissolution only considers the residual weathering-active surface of the eroding material because the effect of preferential dissolution of the congruently dissolved surface is cancelled by the bulk dissolution release of ^{238}U, which will be considered below. Although alpha decay is associated with a long recoiling distance of 10.7 μm for the energetic ^4He nuclei, only the crystal damage associated with the recoiling track of ^{234}Th nuclei is considered because the ^4He with high speed and low mass should only destroy crystal lattices at the very end of its recoiling track (Nasdala et al., 2001). Thus, the damaged crystal lattice caused by the ^{234}Th track is not likely to be connected to that of ^4He. Similar to recoil ejection, only one quarter of the ^{234}U nuclei within the depth of the ^{234}Th recoil track is connected to the mineral surface. The release of ^{234}U associated with preferential dissolution ($^{234}P_A$) of residual weathering-active surface can be expressed as:

$$^{234}P_A = dS_AC_A\lambda_{238}/\lambda_{234}/4 \quad (2)$$

where S_A (L^2) is residual area of weathering-active surface of the eroding materials; and C_A (N/L^3) is the volumetric molar concentration of ^{238}U in the exposed weathering-active minerals. $C_A\lambda_{238}/\lambda_{234}$ reflects the volumetric molar concentration of ^{234}U in weathering-active minerals.

Bulk dissolution is the only source of the ^{238}U nuclei:

$$^{238}D_A = (S_0 - S_A)ZC_A \quad (3)$$

where S_0 (L^2) is the initial area of the exposed weathering-active surface; Z (L) is the average depth of weathering dissolution beneath the surface. The accompanied ^{234}U release associated with bulk dissolution can be derived by:

$$^{234}D_A = {}^{238}D_A\lambda_{238}/\lambda_{234} \quad (4)$$

This relation assumes a (^{234}U/^{238}U) of dissolved minerals in equilibrium and, therefore, implicitly includes the recoil ejection from the surface of weathering-active minerals. There might be some bias of this approach if the weathering-active surface diminished by surface coating also has preferential ^{234}U release either by recoiling or preferential dissolution. However, the effects of both might be minor because 1) the coating, if it is enough to prevent bulk dissolution, might very likely be thicker than the recoiling distance and the active surface diminished by coating may not dominate all of the recoiling surface, and 2) the transport limited of dissolution by coating would also largely inhibit preferential ^{234}U dissolution from the damaged site.

The changing area of weathering active surface through time (t, T), either due to dissolution loss of fine scale surface roughness or due to surface passivation associated with secondary precipitates, is modeled assuming a first-order kinetics:

$$dS_A/dt = -KS_A \quad (5)$$

where K is the dissolution rate constant (T^{-1}). Integrating the above equation gives:

$$S_A = S_0e^{-KT_W} \quad (6)$$

Combining Eqs. (1) to (4) along with Eq. (6) gives:

$$\left(^{234}U/^{238}U\right)_{Riv} = \frac{(^{234}A_{IA} + {}^{234}P_A + {}^{234}D_A)\lambda_{234}}{^{238}D_A\lambda_{238}} = 1 + \frac{R(F\lambda_{234}T_W + e^{-KT_W})}{4(1 - e^{-KT_W})} \quad (7)$$

where F is the fraction of uranium partitioned between weathering-inactive and weathering-active surfaces ($\frac{S_{IA}C_{IA}}{S_0C_A}$), and R is the ratio between recoiling distance (d) and dissolution depth (Z).

Eq. (7) enables $(^{234}U/^{238}U)_{Riv}$ to be related to D because higher T_W is expected under lower D. However, the relationships between D and T_W are not precisely known. Here we use a constant average regolith depth (H, units of L) over which the weathering interfaces are exposed to weathering fluid, based on inverse modeling showing that a constant weathering depth, albeit with considerable range, may be applicable for a wide range of D (West, 2012). For constant depth, the time minerals are exposed to weathering becomes H/D. Replacing T_W in Eq. (7) by H/D gives:

$$\left(^{234}U/^{238}U\right)_{Riv} = 1 + \frac{R(F\lambda_{234}\frac{H}{D} + e^{-K\frac{H}{D}})}{4(1 - e^{-K\frac{H}{D}})} \quad (8)$$

Other relationships, such as exponentially decreasing soil production associated with increasing soil depth (Heimsath et al., 1997), may produce a trend of increasing T_W with decreasing D. However, parameters in these relations are poorly constrained, especially at the global scale and when considering weathering in fractured bedrock as well as overlying mobile regolith. The assumption of constant H thus provides a simplified approach to measure the control exerted by the changing exposure age of the weathering interface on $(^{234}U/^{238}U)_{Riv}$. The potential influence(s) of changing H on $(^{234}U/^{238}U)_{Riv}$ will be discussed in greater detail in the following section.

4.1.3. Model-data fitting

Fitting Eq. (8) to the data in Fig. 1 does not constrain all four free parameters (K, F, R, and H) due to the scatter in the data and the non-linear relationships. Thus, independent constraints on F and H are employed. The ratio of uranium between suspended and dissolved load of rivers can be used to infer the partitioning of uranium between weathering-inactive and weathering-active surfaces, assuming (1) dissolved U represents the total amount of U in weathering-active minerals while the suspended load represents the total amount of weathering-inactive U, and (2) weathering-active and weathering-inactive U-containing minerals have the same volume-specific surface area. Data from global rivers yields a mean $F = 3.60 \pm 1.99$ (2 × standard error; Table S3; Gaillardet et al., 2014), which we take as an upper limit for the mean F value considering the presence in riverine suspended load of some weathering-active minerals and large grains of weathering-inactive minerals that do not contribute to recoil ejection because of their low surface-to-volume ratio. The U partitioning between weathering resistant minerals (e.g., quartz, garnet, rutile, zircon, titanite, and monazite) and weathering unresisting minerals (e.g., biotite, muscovite, magnetite, K-feldspar, carbonate, and apatite) in sediments of Himalayan rivers (Bosia et al., 2018) suggests a lower limit of ~2.3 for F considering that some of the weathering-prone minerals may escape from weathering reaction. We use an F value of 3.0 in the model and consider sensitivity to changing F across a range of 0.95 to 9.5. Inverse modeling between D and W gives a best fit for the weathering depth of 8900 kg/m^2 (West, 2012), which represents H of 3.3 m using a density of 2700 kg/m^3 (density of bedrock is used for calculating denudation rate so that H/D reflects regolith residence time).

Fitting Eq. (8) to data with F of 3.0 and H of 3.3 m successfully reproduces the first-order pattern in changing responses of $(^{234}U/^{238}U)_{Riv}$ to D (Fig. 2a). The regression results in an R of $10^{0.31 \pm 0.18}$ and K of $10^{-3.21 \pm 0.20}$ yr^{-1} (uncertainty reported as 2 × standard error). Considering the nonlinear feature of Eq. (8), the fitting uses the least squares method for a nonlinear regression model in MATLAB software (fitnlm) where the squared residuals are calculated using the logarithm of δ^{234}U, where $\delta^{234}U = [(^{234}U/^{238}U)_{Riv} - 1] \times 1000$. This approach is used because the distribution of $\log(\delta^{234}U)$ in the model is rather uniform while the $(^{234}U/^{238}U)_{Riv}$ is highly skewed toward the equilibrium value. If it were not used, least squares fitting based on $(^{234}U/^{238}U)_{Riv}$ would increase the influence of the catchments with high $(^{234}U/^{238}U)_{Riv}$ value. The goodness of fit of the non-linear model cannot be satisfactorily estimated using parameters such as R-squared that is normally used for linear models. The correlation between the observed and predicted $\log(\delta^{234}U)$ gives a correlation coefficient (r) of 0.77, indicating a fair model prediction. However, the large reduced chi-squared value (χ^2) of 49.8 for the model best-fit suggests that model with fixed parameters cannot fully capture the data, especially for the catchments with $D < 0.6$ mm/yr as can be readily seen in Fig. 2. The deviation of the model and data at low D is discussed in more detail below.

The model also successfully explains the changing variability of $(^{234}U/^{238}U)_{Riv}$ under different D. Sensitivity tests related to the overall fit indicate that, by changing the model parameters by ±0.5 order of magnitude (factors of ~3), variations in H, K, R and F would, in general, result in larger changes of $(^{234}U/^{238}U)_{Riv}$ for the catchments with high and low D (Fig. 3). A higher K may partly explain the lower $(^{234}U/^{238}U)_{Riv}$ in the catchments on the west coast of South Island, New Zealand compared to the relatively drier catchments on the eastern slopes of the Southern Alps with similar D (Robinson et al., 2004a).

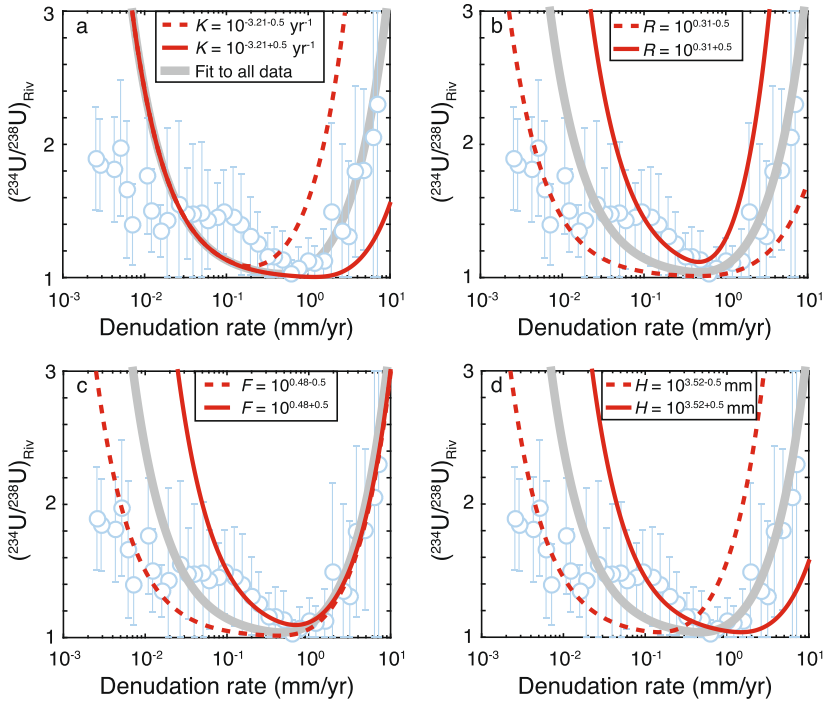

Fig. 3. Sensitivity tests showing different modeled behavior of $(^{234}U/^{238}U)_{Riv}$ for (a) changing decay rate constant of weathering-active surface (K), (b) ratio between recoil distance and surface dissolution depth (R), (c) surface partition of uranium between weathering inactive and active minerals (F), and (d) average depth where the weathering surface is generated (H). Error bars depict standard deviation within each averaging bin.

4.2. Implication for weathering depth

The model generally fits the data well for catchments with high D but less well for those with low D. This is caused by the muted response of $(^{234}U/^{238}U)_{Riv}$ to D for catchments with D between 0.02 and 0.09 mm/yr. The reason for the muted response under low D is unclear. Longer residence time of water in the watershed with low D could in part explain why there is lower $(^{234}U/^{238}U)_{Riv}$ than the prediction, i.e., long water residence time allows dissolved ratios to return towards secular equilibrium. Sensitivity analyses (Fig. 3) suggest that changing R, F, and H values with D may also contribute. The partitioning of uranium between weathering-active and weathering-inactive surfaces is largely determined by lithology. Thus, there is no *a priori* reason F should systematically decrease with decreasing D. The ratio between recoiling distance and dissolution depth (R) may be related to lithology (mineral type) and environmental factors such as temperature. However, there is also no *a priori* reason that these factors should change systematically with D.

We propose that lower $(^{234}U/^{238}U)_{Riv}$ than predicted at low D may be related to changes in H, the length scale over which weathering interfaces are exposed. Bare rock typically dominates the surface of catchments with high D because regolith is poorly developed owing to limited exposure time and the dominance of landslides in the total erosional flux (Hovius et al., 1997). Although a patchy soil mantle may still be observed (Larsen et al., 2014), the interfaces that contribute to the weathering reaction at high D are mainly from deep fractures in bedrock (Calmels et al., 2011; West, 2012). In contrast, at low D, well-developed regolith at shallow depth provides most of the active weathering interface, instead of deep fractures.

Fitting the model to catchments with $D > 0.09$ mm/yr gives values of $10^{3.92 \pm 0.40}$ mm (8.3 m), $10^{0.45 \pm 0.42}$, and $10^{-3.45 \pm 0.63}$ yr^{-1} for H, R, and K, respectively ($r = 0.93$, $\chi^2 = 1.2$, Fig. 2a). The regressed values of R and K are very similar to the overall regression, i.e., when including all data. However, fitting the model for only the data with $D < 0.02$ mm/yr does not give good constraints on the values of H, R, and K because of the scattered dataset. Thus, to illustrate the possible changing H in response to changing hillslope processes, fixed R of $10^{0.45}$ and K of $10^{-3.45}$ yr^{-1} derived from the model fitting for catchments with $D > 0.09$ mm/yr are used. For these parameters, the model gives H of $10^{2.86 \pm 0.13}$ mm (0.72 m) for the catchments with $D < 0.02$ mm/yr ($r = 0.77$, $\chi^2 = 8.1$, Fig. 2a). An H value of 0.72 m is typical of the length scale of weathering fronts observed in well-developed regolith (White and Buss, 2014). Thus, the $(^{234}U/^{238}U)_{Riv}$ data could be explained if the length scale of weathering differs at low D ($H = 0.72$ m), when most weathering takes place in well-developed regolith, versus at high D ($H = 8.3$ m), when significant weathering takes place in deep fractures.

4.3. Implication for weathering regimes and uranium comminution age

The relatively good fit between Eq. (8) and the data, both in overall trend and in variability, indicates control of shifting weathering regime on $(^{234}U/^{238}U)_{Riv}$. Shifting weathering regime can also be illustrated by fraction of the exposed weathering-active surface that have dissolved (f_W). According to the model, dependence of f_W on D can be derived from Eq. (6):

$$f_W = \frac{S_A}{S_0} = 1 - e^{-K\frac{H}{D}} \tag{9}$$

Using the regressed values of K, Eq. (9) indicates that most of the exposed weathering-active minerals have been dissolved as $(^{234}U/^{238}U)_{Riv}$ approaches its minimum value (Fig. 2b), i.e., when weathering shifts from a supply-limited to kinetically-limited regime.

The $(^{234}U/^{238}U)_{Riv}$ data may provide some quantitative information about the shift in weathering regime. At low D, if most weathering takes place in a relatively narrow zone in the regolith such that $H = 0.72$ m, then the model indicates shifting weathering regimes at an average D of ~0.07 mm/yr. Considering the rather scattered nature of all of the $(^{234}U/^{238}U)_{Riv}$ data

and the average, we expect a rather wide ranges for the threshold D between supply-limited and kinetically-limited weathering regimes in response to changing climate, lithology, etc. Nevertheless, the average threshold D constrained for the supposed landscapes dominated surface weathering interfaces is slightly higher than that derived from the correlation between D and W in granitic catchments (~0.04 mm/yr in average), where W was calculated as the cation flux from silicate minerals (West, 2012; West et al., 2005). This slight discrepancy might be caused by the high dissolution rate of the weathering-active U-containing minerals such as apatite when compared to silicate minerals.

For higher D, when weathering may be primarily occurring at depth with $H = 8.3$ m, the shift from supply to kinetic limits on $(^{234}U/^{238}U)$ occurs at $D \sim 0.8$ mm/yr is suggested. But this transition point does not imply that all of the minerals have been dissolved for catchments with $D < 0.8$ mm/yr, as in the case of truly supply-limited weathering in the sense defined for total weathering fluxes (e.g., West et al., 2005). The shifting weathering regime recorded in U isotopes may only reflect the weathering intensity of the exposed weathering interface, and a large quantity of rock can still escape from weathering reactions by rapid mass wasting and erosional transport of unweathered large grains without exposed surfaces.

Decreasing $(^{234}U/^{238}U)_{Riv}$ is related to decreasing D under a kinetically-limited weathering regime, while increasing $(^{234}U/^{238}U)_{Riv}$ with decreasing D indicates a supply-limited weathering regime. During the incipient stage of weathering, the surface area of weathering-active minerals is high. Thus, high $(^{234}U/^{238}U)_{Riv}$ is produced because of the preferential release of ^{234}U from the damaged lattices relative to limited bulk dissolution of weathering-active minerals that release ^{234}U and ^{238}U stoichiometrically. Increasing weathering intensity in response to decreasing D decreases $(^{234}U/^{238}U)_{Riv}$ by increasing the bulk dissolution of ^{234}U and ^{238}U (releasing these at their secular equilibrium ratio) while the preferential release of ^{234}U decreases due to the decreasing surface area (volume) of weathering-active minerals. At a low denudation rate, the exposed weathering-active minerals have been totally consumed. Progressive loss of the recoil-ejected ^{234}U from the weathering-inactive minerals, with more lost as minerals reside longer in the weathering zone, results in increasing $(^{234}U/^{238}U)_{Riv}$ values with decreasing D.

The time scale for shifting weathering regime can provide constraints on the influence of weathering on uranium comminution ages, which have attracted recent attention (DePaolo et al., 2012, 2006; Dosseto et al., 2010; Li et al., 2017b). The calculation of uranium comminution age for sediment is based on recoil-driven depletion of ^{234}U on the mineral surface through time. Preferential dissolution of ^{234}U from radioactively-damaged sites would biases calculated comminution ages (DePaolo et al., 2012). Complete dissolution (>95%) of weathering-active surfaces at D of ~0.8 mm/yr and ~0.07 mm/yr for deep fracture dominated ($H = \sim 8.3$ m) and surface regolith dominated ($H = \sim 0.72$ m) landscapes corresponds to a weathering interface age of ~10 kyrs. Considering the rather long half-life of ^{234}U of 245.6 kyrs (Cheng et al., 2013) and the precision of uranium isotope measurement (~1 ‰), uranium comminution age calculations are mainly applied to systems with ages that are older than ~10 kyrs. Thus, the complete dissolution of the exposed weathering-active surfaces on a time scale of ~10 kyrs implies that preferential ^{234}U dissolution should have a negligible influence on the calculation of uranium comminution age, and the uranium comminution age method should mainly reflect that of the weathering-inactive mineral surfaces.

4.4. Field-to-laboratory discrepancy in mineral dissolution rate

The regressed values of K and R have important implications for the discrepancy between mineral dissolution rates observed in the field and in laboratory experiments. Sensitivity tests show that $(^{234}U/^{238}U)_{Riv}$ is most sensitive to K, H and R, but not to F, under high D (Fig. 3). Thus, regressions based on the catchments with $D > 0.09$ mm/yr, with K, H, and R as free parameters, should give a relatively good constraint on K *and* R, with good χ^2 (1.2) and with little expected bias from the fixed F value. The regressed R of $10^{0.45}$, indicate an average surface dissolution depth (Z) of 7.4 nm using a d value of about 20.8 nm (Nasdala et al., 2001). The shallow dissolution depth may be caused by surface passivation due to secondary precipitation or the dominance of fine scale roughness in the weathering interfaces. The regressed K *and* R gives apparent dissolution rate of $10^{-2.58}$ nm/yr (i.e., $K \times d/R$). However, since K and R are not independent in the model fitting procedure, the error on apparent dissolution rate cannot be propagated from those of K and R directly. Instead, using dissolution rate as a modeling parameter, and calculating the K from dissolution rate and R, would give an apparent dissolution rate of $10^{-2.58 \pm 0.23}$ nm/yr.

Comparing the regressed best-fit dissolution rate of $10^{-2.58 \pm 0.23}$ nm/yr to other dissolution rate data needs to consider the effect of surface area scale, because most field and laboratory dissolution rates are normalized to BET surface area. The BET method measures surface area based on absorption of N_2, which has a scale (~0.35 nm) that is much finer than the ^{234}Th recoiling distance of ~20.8 nm. Thus, the N_2-based BET method would capture a greater proportion of the local scale roughness, and consequently higher specific surface areas and lower dissolution rates are expected when compared to those associated with ^{234}U loss by recoil (Aciego et al., 2011; Bourdon et al., 2009). According to the scaling law established for basalt weathering (Navarre-Sitchler and Brantley, 2007), a BET-normalized site-specific dissolution rate of $10^{-3.17 \pm 0.23}$ nm/yr is estimated, based on the best-fit dissolution rate from the $^{234}U/^{238}U$ data (note that the error introduced by BET-normalization is not considered).

This BET-normalized site-specific dissolution rate of $10^{-3.17 \pm 0.23}$ nm/yr confirms the large discrepancy between field rates and laboratory rates (e.g., Brantley and Olsen, 2014; White and Brantley, 2003). According to the U partitioning in sediments from Himalayan rivers, the predominant U-containing weathering-active minerals include biotite, muscovite, magnetite, K-feldspar, carbonate, and apatite (Bosia et al., 2018). BET surface area normalized dissolution rates of these minerals, derived from depletion in regolith profiles (White and Brantley, 2003; White and Buss, 2014), range from $10^{-4.50}$ to $10^{-0.30}$ nm/yr (Fig. 4, Table S4). These field-derived mineral dissolution rates are very similar to the BET-normalized site-specific dissolution rate constrained by this work. Overestimation of active surface area due to surface passivation and reduction of energetically active sites has been proposed as an intrinsic reason for the low dissolution rates observed in the field (White and Brantley, 2003). The site-specific dissolution rate from the $^{234}U/^{238}U$ model reflects the intrinsic dissolution rate of the exposed weathering-active sites, and thus is independent of the estimated active surface area that may be influenced by surface passivation for example due to secondary precipitates (White and Brantley, 2003). Thus, the consistency between the dissolution rate inferred from the $^{234}U/^{238}U$ model and from other field dissolution rate data suggests that the low dissolution rate observed in the field may be caused by extrinsic factors related to chemical affinity of the weathering fluid. Stagnant micro-pores, slow flow rates associated with low permeability, and low water/rock ratios may produce weathering fluids that are closer to equilibrium at the mineral surface in field settings when compared to lab experiments (White and Brantley, 2003;

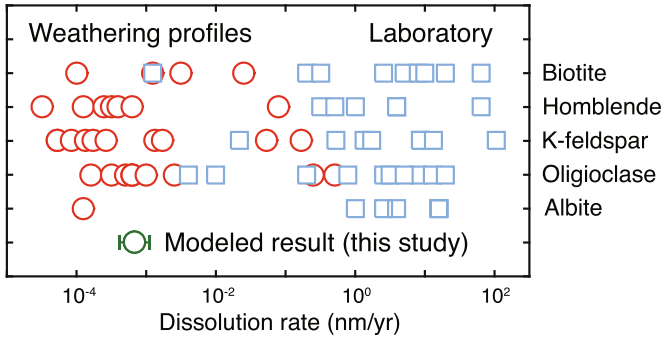

Fig. 4. Comparing the site-specific mineral dissolution rate constrained by the relationship between $(^{234}U/^{238}U)_{Riv}$ and D to those estimated from field weathering profiles in regolith and laboratory experiments. Red points on the left side are the BET surface area normalized field dissolution rates from: White and Brantley (2003), White and Buss (2014). The blue squares on the right side are the dissolution rates based on laboratory experiments. Data source: White and Brantley (2003). Error bars show 2 × standard error (2SE) of the model result.

White and Buss, 2014), and, therefore, result in low dissolution rate.

5. Conclusion

A global data compilation including new measurements from Chinese rivers reveals changing responses of riverine dissolved $(^{234}U/^{238}U)$ ratio, both in mean value and variability, to catchment-scale denudation rate. Changing responses of $(^{234}U/^{238}U)_{Riv}$ to D can be explained by the competing uranium release from weathering-active and weathering-inactive surfaces associated with shifting weathering regimes, providing independent evidence to corroborate the distinction between supply- and kinetically-limited regimes. Higher variability of $(^{234}U/^{238}U)_{Riv}$ for the catchments with high and low D values may reflect natural variation of decay rate of weathering surface, depth of surface dissolution, surface partition of uranium between weathering-active and weathering-inactive minerals, and exposure depth of the weathering interface. A much deeper exposure depth of weathering interface (~8.3 m) is suggested for catchments with $D >$ 0.09 mm/yr compared to those (~0.72 m) for catchments with $D <$ 0.02 mm/yr. The deeper weathering interface might be related to a higher contribution of weathering products from deep fractures at high D compared to landscapes where well-developed regolith at shallow depths contributes most of the weathering flux. In both cases, complete consumption of the exposed weathering-active surface, and thus transition from kinetically-limited to supply-limited weathering regime, is estimated to occur at ~10 kyrs. Thus, the uranium comminution age of sediment, which is mainly applied to timescales much longer than 10 kyrs, is controlled by weathering-inactive surfaces and the influence of weathering dissolution is likely to be limited. A BET normalized site-specific dissolution rate of $10^{-3.17 \pm 0.23}$ nm/yr is constrained, such that $(^{234}U/^{238}U)$ data are consistent with the large discrepancy between weathering rates observed in field and laboratory settings. Since the site-specific dissolution rate derived from $(^{234}U/^{238}U)$ reflects the intrinsic dissolution rate, the high degree of chemical equilibrium of weathering fluid at weathering sites caused by stagnant micro-pores, low flow rate, and high rock/water ratio is suggested to explain the low field dissolution rate observed instead of the passivation of mineral surface due to secondary precipitates.

Acknowledgements

Reviews by Dr. Anthony Dosseto and two other anonymous reviewers largely helped to improve an early version of the manuscript. Ruo-Mei Wang is thanked for her help with information of Taiwan samples and the uranium isotope method. This work was supported by the Natural Science Foundation of China (Nos. 41730101, 41761144058 and 41711530222) and National Research Foundation – South Africa (No. 110777).

Appendix A. Supplementary material

Supplementary material related to this article can be found online at https://doi.org/10.1016/j.epsl.2018.08.008.

References

Aciego, S., Bourdon, B., Schwander, J., Baur, H., Forieri, A., 2011. Toward a radiometric ice clock: uranium ages of the Dome C ice core. Quat. Sci. Rev. 30, 2389–2397.
Andersen, M.B., Erel, Y., Bourdon, B., 2009. Experimental evidence for ^{234}U–^{238}U fractionation during granite weathering with implications for $^{234}U/^{238}U$ in natural waters. Geochim. Cosmochim. Acta 73, 4124–4141.
Andersen, M.B., Stirling, C.H., Zimmermann, B., Halliday, A.N., 2010. Precise determination of the open ocean $^{234}U/^{238}U$ composition. Geochem. Geophys. Geosyst. 11.
Bagard, M.-L., Chabaux, F., Pokrovsky, O.S., Viers, J., Prokushkin, A.S., Stille, P., Rihs, S., Schmitt, A.-D., Dupré, B., 2011. Seasonal variability of element fluxes in two Central Siberian rivers draining high latitude permafrost dominated areas. Geochim. Cosmochim. Acta 75, 3335–3357.
Berner, R., Lasaga, A., Garrells, R., 1983. The carbonate–silicate geochemical cycle and its effect on atmospheric carbon dioxide over the past 100 million years. Am. J. Sci. 283, 641–683.
Bluth, G.J.S., Kump, L.R., 1994. Lithologic and climatologic controls of river chemistry. Geochim. Cosmochim. Acta 58, 2341–2359.
Bosia, C., Chabaux, F., Pelt, E., Cogez, A., Stille, P., Deloule, E., France-Lanord, C., 2018. U-series disequilibria in minerals from Gandak River sediments (Himalaya). Chem. Geol. 477, 22–34.
Bourdon, B., Bureau, S., Andersen, M.B., Pili, E., Hubert, A., 2009. Weathering rates from top to bottom in a carbonate environment. Chem. Geol. 258, 275–287.
Brantley, S.L., Olsen, A.A., 2014. Reaction kinetics of primary rock-forming minerals under ambient conditions. In: Treatise on Geochemistry, second edition. Elsevier, Oxford, pp. 69–113.
Calmels, D., Galy, A., Hovius, N., Bickle, M., West, A.J., Chen, M.-C., Chapman, H., 2011. Contribution of deep groundwater to the weathering budget in a rapidly eroding mountain belt, Taiwan. Earth Planet. Sci. Lett. 303, 48–58.
Cermeño, P., Falkowski, P.G., Romero, O.E., Schaller, M.F., Vallina, S.M., 2015. Continental erosion and the Cenozoic rise of marine diatoms. Proc. Natl. Acad. Sci. 112, 4239–4244.
Chabaux, F., Riotte, J., Clauer, N., France-Lanord, C., 2001. Isotopic tracing of the dissolved U fluxes of Himalayan rivers: implications for present and past U budgets of the Ganges–Brahmaputra system. Geochim. Cosmochim. Acta 65, 3201–3217.
Chabaux, F., Riotte, J., Dequincey, O., 2003. U–Th–Ra fractionation during weathering and river transport. Rev. Mineral. Geochem. 52, 533–576.
Cheng, H., Lawrence Edwards, R., Shen, C.-C., Polyak, V.J., Asmerom, Y., Woodhead, J., Hellstrom, J., Wang, Y., Kong, X., Spötl, C., Wang, X., Calvin Alexander, E., 2013. Improvements in ^{230}Th dating, ^{230}Th and ^{234}U half-life values, and U–Th isotopic measurements by multi-collector inductively coupled plasma mass spectrometry. Earth Planet. Sci. Lett. 371–372, 82–91.
Dellinger, M., Gaillardet, J., Bouchez, J., Calmels, D., Louvat, P., Dosseto, A., Gorge, C., Alanoca, L., Maurice, L., 2015. Riverine Li isotope fractionation in the Amazon River basin controlled by the weathering regimes. Geochim. Cosmochim. Acta 164, 71–93.
DePaolo, D.J., Lee, V.E., Christensen, J.N., Maher, K., 2012. Uranium comminution ages: sediment transport and deposition time scales. C. R. Géosci. 344, 678–687.
DePaolo, D.J., Maher, K., Christensen, J.N., McManus, J., 2006. Sediment transport time measured with U-series isotopes: results from ODP North Atlantic drift site 984. Earth Planet. Sci. Lett. 248, 394–410.
Dosseto, A., Hesse, P.P., Maher, K., Fryirs, K., Turner, S., 2010. Climatic and vegetation control on sediment dynamics during the last glacial cycle. Geology 38, 395–398.
Dosseto, A., Turner, S.P., Douglas, G.B., 2006. Uranium-series isotopes in colloids and suspended sediments: timescale for sediment production and transport in the Murray–Darling River system. Earth Planet. Sci. Lett. 246, 418–431.
Dunk, R.M., Mills, R.A., Jenkins, W.J., 2002. A reevaluation of the oceanic uranium budget for the Holocene. Chem. Geol. 190, 45–67.
Emberson, R., Hovius, N., Galy, A., Marc, O., 2016. Oxidation of sulphides and rapid weathering in recent landslides. Earth Surf. Dyn. 4, 727–742.
Ferrier, K.L., Riebe, C.S., Hahm, W.J., 2016. Testing for supply-limited and kinetic-limited chemical erosion in field measurements of regolith production and chemical depletion. Geochem. Geophys. Geosyst. 17, 2270–2285.
Fleischer, R.L., 1980. Isotopic disequilibrium of uranium: alpha-recoil damage and preferential solution effects. Science 207, 979–981.

Gabet, E.J., Mudd, S.M., 2009. A theoretical model coupling chemical weathering rates with denudation rates. Geology 37, 151–154.
Gaillardet, J., Viers, J., Dupré, B., 2014. Trace elements in river waters. In: Treatise on Geochemistry, second edition. Elsevier, Oxford, pp. 195–235.
Heimsath, A., Dietrich, W.E., Nishiizumi, K., Finkel, R., 1997. The soil production function and landscape equilibrium. Nature 388, 358–361.
Hilley, G.E., Chamberlain, C.P., Moon, S., Porder, S., Willett, S.D., 2010. Competition between erosion and reaction kinetics in controlling silicate-weathering rates. Earth Planet. Sci. Lett. 293, 191–199.
Hovius, N., Stark, C.P., Allen, P.A., 1997. Sediment flux from a mountain belt derived by landslide mapping. Geology 25, 231–234.
Jacobson, A.D., Blum, J.D., Chamberlain, C.P., Craw, D., Koons, P.O., 2003. Climatic and tectonic controls on chemical weathering in the New Zealand Southern Alps. Geochim. Cosmochim. Acta 67, 29–46.
Jaffey, A.H., Flynn, K.F., Glendenin, L.E., Bentley, W.C., Essling, A.M., 1971. Precision measurement of half-lives and specific activities of ^{235}U and ^{238}U. Phys. Rev. C 4, 1889–1906.
Jasechko, S., Perrone, D., Befus, K.M., Cardenas, M.B., Ferguson, G., Gleeson, T., Luijendijk, E., Mcdonnell, J.J., Taylor, R.G., Wada, Y., 2017. Global aquifers dominated by fossil groundwaters but wells vulnerable to modern contamination. Nat. Geosci. 10, 425–429.
Kigoshi, K., 1971. Alpha-recoil thorium-234: dissolution into water and the uranium-234/uranium-238 disequilibrium in nature. Science 173, 47–48.
Kronfeld, J., Vogel, J.C., 1991. Uranium isotopes in surface waters from southern Africa. Earth Planet. Sci. Lett. 105, 191–195.
Larsen, I.J., Almond, P.C., Andre, E., Stone, J.O., Montgomery, D.R., Brendon, M., 2014. Rapid soil production and weathering in the Southern Alps, New Zealand. Science 343, 637–640.
Li, G., Elderfield, H., 2013. Evolution of carbon cycle over the past 100 million years. Geochim. Cosmochim. Acta 103, 11–25.
Li, G., Hartmann, J., Derry, L.A., West, A.J., You, C.-F., Long, X., Zhan, T., Li, L., Li, G., Qiu, W., Li, T., Liu, L., Chen, Y., Ji, J., Zhao, L., Chen, J., 2016. Temperature dependence of basalt weathering. Earth Planet. Sci. Lett. 443, 59–69.
Li, G., West, A.J., Densmore, A.L., Jin, Z., Zhang, F., Wang, J., Clark, M., Hilton, R.G., 2017a. Earthquakes drive focused denudation along a tectonically active mountain front. Earth Planet. Sci. Lett. 472, 253–265.
Li, L., Liu, X., Li, T., Li, L., Zhao, L., Ji, J., Chen, J., Li, G., 2017b. Uranium comminution age tested by the eolian deposits on the Chinese Loess Plateau. Earth Planet. Sci. Lett. 467, 64–71.
Maher, K., Chamberlain, C.P., 2014. Hydrologic regulation of chemical weathering and the geologic carbon cycle. Science 343, 1502–1504.
Maher, K., DePaolo, D.J., Christensen, J.N., 2006. U–Sr isotopic speedometer: fluid flow and chemical weathering rates in aquifers. Geochim. Cosmochim. Acta 70, 4417–4435.
Nasdala, L., Wenzel, M., Vavra, G., Irmer, G., Wenzel, T., Kober, B., 2001. Metamictisation of natural zircon: accumulation versus thermal annealing of radioactivity-induced damage. Contrib. Mineral. Petrol. 141, 125–144.
Navarre-Sitchler, A., Brantley, S., 2007. Basalt weathering across scales. Earth Planet. Sci. Lett. 261, 321–334.
Perron, J.T., 2017. Climate and the pace of erosional landscape evolution. Annu. Rev. Earth Planet. Sci. 45, 561–591.
Pogge Von Strandmann, P.A.E., Henderson, G.M., 2015. The Li isotope response to mountain uplift. Geology 43.
Raymo, M., Ruddiman, W.F., Froelich, P.N., 1988. Influence of Late Cenozoic mountain building on ocean geochemical cycles. Geology 16, 649–653.
Riebe, C.S., Kirchner, J.W., Finkel, R.C., 2004. Erosional and climatic effects on long-term chemical weathering rates in granitic landscapes spanning diverse climate regimes. Earth Planet. Sci. Lett. 224, 547–562.
Robinson, L.F., Henderson, G.M., Hall, L., Matthews, I., 2004a. Climatic control of riverine and seawater uranium-isotope ratios. Science 305, 851–854.
Robinson, L.F., Belshaw, N.S., Henderson, G.M., 2004b. U and Th concentrations and isotope ratios in modern carbonates and waters from the Bahamas. Geochim. Cosmochim. Acta 68, 1777–1789.
Vigier, N., 2001. Erosion timescales derived from U-decay series measurements in rivers. Earth Planet. Sci. Lett. 193, 549–563.
Vigier, N., Burton, K.W., Gislason, S.R., Rogers, N.W., Duchene, S., Thomas, L., Hodge, E., Schaefer, B., 2006. The relationship between riverine U-series disequilibria and erosion rates in a basaltic terrain. Earth Planet. Sci. Lett. 249, 258–273.
Wang, R.M., You, C.F., 2013. Precise determination of U isotopic compositions in low concentration carbonate samples by MC-ICP-MS. Talanta 107, 67–73.
West, A.J., 2012. Thickness of the chemical weathering zone and implications for erosional and climatic drivers of weathering and for carbon-cycle feedbacks. Geology 40, 811–814.
West, A.J., Galy, A., Bickle, M., 2005. Tectonic and climatic controls on silicate weathering. Earth Planet. Sci. Lett. 235, 211–228.
White, A.F., Brantley, S.L., 2003. The effect of time on the weathering of silicate minerals: why do weathering rates differ in the laboratory and field? Chem. Geol. 202, 479–506.
White, A.F., Buss, H.L., 2014. Natural weathering rates of silicate minerals. In: Treatise on Geochemistry, second edition. Elsevier, Oxford, pp. 115–155.